J. Fluid Mech. (2004), *vol.* 518, *pp.* 363–379.
DOI: 10.1017/S0022112004001119 Printed in the United Kingdom

Spatio-temporal instability of the natural-convection boundary layer in thermally stratified medium

By J. TAO†, P. LE QUÉRÉ AND S. XIN

LIMSI-CNRS, BP133, 91403 Orsay Cedex, France

(Received 9 January 2003 and in revised form 5 July 2004)

This paper investigates the spatio-temporal instability of the natural-convection boundary-layer flow adjacent to a vertical heated flat plate immersed in a thermally stratified ambient medium. The temperature on the plate surface is distributed linearly. By introducing a temperature gradient radio a between the wall and the medium, we obtain a similarity solution which can describe in a smooth way the evolution between the states with isothermal and uniform-heat-flux boundary conditions. It is shown that the flow reversal in the basic flow vanishes when a is larger than a critical value. A new absolute–convective instability transition of this flow is identified in the context of the coupled Orr–Sommerfeld and energy equations. Increasing a decreases the domain of absolute instability, and when a is large enough the absolute instability disappears. In particular, when $a = 0$ (isothermal surface), the interval of absolute instability becomes narrower for fluids of larger Prandtl numbers, and the absolute instability does not occur for Prandtl numbers greater than 70; when $a = 1$ (uniform-heat-flux surface) the instability remains convective in a wide Prandtl number range. Analysis of the Rayleigh equations for this problem reveals that the basic flows supporting this new instability transition have inviscid origin of convective instability. Based on the steep global mode theory, the effects of a and Prandtl number on the global frequency are discussed as well.

1. Introduction

For natural convection flows over a heated vertical or inclined plate, the temperature distribution on the surface and the thermal stratification in the ambient medium define the main characteristics of the flow field and play important roles in producing instabilities. The inclined case was first investigated by Prandtl (1952) to simulate 'mountain and valley winds in stratified air'. The ambient fluid was assumed to be linearly stratified and kept at a constant horizontal temperature difference from the wall. Due to the background stratification, a temperature defect and flow reversal were found in the boundary layer. Iyer (1973) and Iyer & Kelly (1978) studied the Prandtl buoyancy boundary-layer solution based on linear and weakly nonlinear stability analysis respectively. The neutral curves for various angles of inclination were calculated, and only supercritical finite-amplitude wave solutions were obtained. In order to simulate vertical 'buoyancy' layers in a heated rectangular cavity, Gill (1966)

† Author to whom correspondence should be addressed; present address: Department of Earth Sciences, University of Cambridge, Madingley Road, Cambridge, CB3 0EZ, UK. jt336@cam.ac.uk

provided an exact solution where the wall and ambient fluid have the same linear temperature gradients. One interesting result of the solution is that the corresponding flow is parallel and simply one-dimensional both for velocity and temperature fields. Based on this solution Gill & Davey (1969) determined the neutral stability conditions for a wide range of Prandtl numbers. Jaluria & Gebhart (1974) studied theoretically and experimentally a boundary layer whose temperature difference between the wall and the extensive medium varied downstream with a power-law $x^{0.2}$. The exponent guarantees that the wall will dissipate a uniform heat flux. They revealed that a stable ambient stratification delayed the onset of transition. Their velocity and temperature fields were confirmed by a later numerical study of Jaluria & Himasekhar (1983) via a finite difference method. Kulkarni, Jacobs & Hwang (1987) obtained a similarity solution describing the boundary layer around an isothermally heated plate, which was used later by Krizhevsky, Cohen & Tanny (1996) in their linear instability analysis. To the best of our knowledge, only the isothermal and uniform-heat-flux boundary conditions have been studied in past theoretical work and until now there have been no other similarity solutions for such buoyancy-driven flow because of the difficulties due to the stratified ambient medium.

Linear stability analysis has been proven a powerful tool to describe the first stage to turbulence. Its main object is to determine the complex wavenumbers and frequencies of infinitesimal wave perturbations that a system supports, because the imaginary parts of the wavenumbers and frequencies represent spatial and temporal growth (or decay) rates, respectively. In most past studies of natural-convection boundary layers, either a purely temporal analysis (the imaginary part of the wavenumber is set zero) or a purely spatial analysis (the frequency is taken as real) was done, but it is well known that the disturbances sometimes experience spatio-temporal propagation in the downstream direction. Consequently, the concepts of absolute and convective instabilities turnout to be of great important in understanding the corresponding physical mechanism. In convectively unstable flow the amplified disturbances move away from the source and in the absolutely unstable case the disturbances will eventually contaminate the entire flow. The distinction requires a fully spatio-temporal analysis, which was first used in plasma instability (Briggs 1964), and more recently applied to natural-convection flows (Krizhevsky *et al.* 1996; Tao & Zhuang 2000). Gaster (1968) investigated laminar flat-plate boundary layer flow and found the transient response to correspond to convective instability. Recently Moresco & Healey (2000) studied the mixed-convection boundary layer over a semi-infinite vertical isothermal plate, and found that the flow became absolutely unstable when the reverse flow caused by the opposite external flow extended over a critical value, where artificial velocity profiles were used to simulate the flow field beyond the separation point of the boundary layer. Based on a special case of Kulkarni *et al.*'s (1987) solution – a medium with linear thermal stratification – Krizhevsky *et al.* (1996) analysed the linear instability of a boundary layer and found that the flow changed from convectively unstable into absolutely unstable at a critical Grashof number which increased with the Prandtl number. Compared with other spatially developing flows, such as wakes, mixing layers and jets where the relations between local (convective/absolute) and global instabilities have been studied widely and profoundly (see Huerre & Monkewitz 1990 for a review), the corresponding study for flat-plate boundary-layer flows is still rudimentary, and this is the principal motivation behind the present study.

The boundary-layer flow to be considered here differs from those above in that the vertical heated wall and the ambient fluid have independent vertical temperature

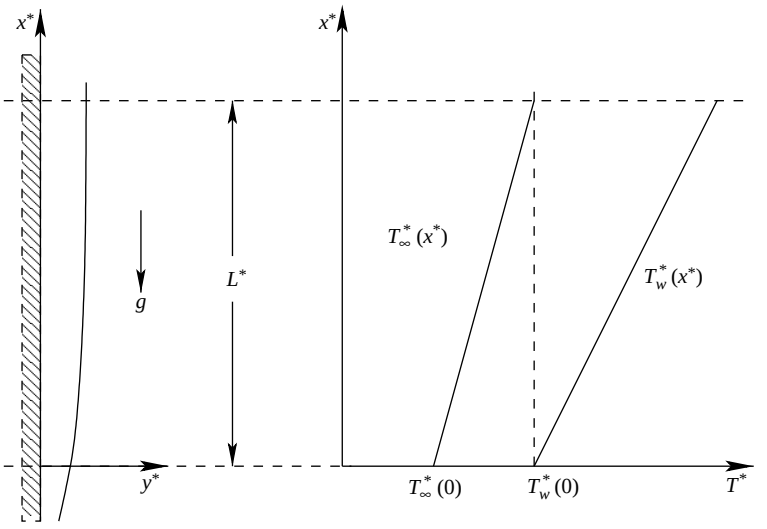

FIGURE 1. Schematic of the coordinate system and temperature distributions on the wall and in the ambient medium.

gradients. After introducing a ratio between the temperature gradients we obtain a similarity solution, by which a variety of cases from the isothermal to the uniform-heat-flux boundary conditions can be analysed within a single framework. The paper is organized as follows: § 2 gives the governing equations and methods of solution. Section 3 discusses the effects of the temperature gradient ratio on the critical instability. In § 4 a new absolute–convective local instability transition is revealed, and then the effects of the Prandtl number and the gradient ratio on the transition are analysed. The global instability is discussed in § 5 and, finally, conclusions are presented in § 6.

2. Governing equations and methods

Consider a buoyancy-driven flow adjacent to a heated vertical plate, which is immersed in thermally stratified fluid with a temperature gradient $N_\infty > 0$. The surface temperature increases independently and linearly in the downstream direction with a gradient $N \geqslant 0$. The streamwise coordinate x^* is measured vertically and opposite to the direction of gravitational acceleration g, and y^* is the coordinate normal to the surface (stars indicate dimensional quantities). The heated wall is assumed to be of finite extent, and its temperature is above that of the surrounding fluid at any elevation (figure 1). The temperature distributions on the wall and in the ambient fluid are given by

$$T^*_w(x) = T^*_w(0) + Nx^*, \quad T^*_\infty(x) = T^*_\infty(0) + N_\infty x^*, \quad T^*_w(0) - T^*_\infty(0) > 0, \quad a = N/N_\infty \tag{2.1a}$$

where the subscript '∞' denotes the ambient condition, and $T^*_w(0) - T^*_\infty(0)$ is the temperature difference between the wall and the background fluid at $x^* = 0$. L^* is a long length scale where $T^*_\infty(L^*) = T^*_w(0)$, and a is the temperature gradient ratio.

The non-dimensional variables employed here are defined as

$$\left.\begin{aligned} &Gr=\left(\frac{g\beta(T_w^*(0)-T_\infty^*(0))L^{*3}}{\nu^2}\right)^{1/4}, \quad (X,Y)=\frac{(x^*,y^*)Gr}{L^*}, \quad (U,V)=(u^*,v^*)\frac{L^*}{\nu Gr^2},\\ &\tau=\frac{\tau^*}{L^{*2}}\nu Gr^3, \qquad \phi=\frac{T^*-T_\infty^*(x^*)}{T_w^*(x^*)-T_\infty^*(x^*)}, \qquad P=\frac{P^*-P_\infty^*(x^*)}{\rho\nu^2Gr^4}L^{*2}, \end{aligned}\right\} \tag{2.1b}$$

where ρ is the fluid density, (u^*, v^*) the base flow velocity components in the (x^*, y^*) directions, p^* the pressure, τ^* the time, Gr the Grashof number, ν the kinematic viscosity and β the coefficient of thermal expansion.

Employing the Boussinesq approximation, taking the remaining properties as constants and neglecting the viscous dissipation, we obtain the governing equations

$$\left.\begin{aligned} &\frac{\partial U}{\partial X}+\frac{\partial V}{\partial Y}=0,\\ &\frac{\partial U}{\partial \tau}+U\frac{\partial U}{\partial X}+V\frac{\partial U}{\partial Y}=-\frac{\partial P}{\partial X}+\frac{1}{Gr}\nabla^2U+\frac{1}{Gr}\phi\,[1+(a-1)\varepsilon X],\\ &\frac{\partial V}{\partial \tau}+U\frac{\partial V}{\partial X}+V\frac{\partial V}{\partial Y}=-\frac{\partial P}{\partial Y}+\frac{1}{Gr}\nabla^2V,\\ &\frac{\partial \phi}{\partial \tau}+U\frac{\partial \phi}{\partial X}+V\frac{\partial \phi}{\partial Y}=\frac{1}{PrGr}\nabla^2\phi-\frac{U\varepsilon\,[1+(a-1)\phi]}{1+(a-1)\varepsilon X}+\frac{2}{PrGr}\frac{\partial \phi}{\partial X}\varepsilon(a-1), \end{aligned}\right\} \tag{2.2a}$$

with boundary conditions

$$U(\tau,X,0)=V(\tau,X,0)=1-\phi(\tau,X,0)=\phi(\tau,X,\infty)=U(\tau,X,\infty)=P(\tau,X,\infty)=0, \tag{2.2b}$$

where the operator $\nabla^2=\partial^2/\partial X^2+\partial^2/\partial Y^2$, the Prandtl number $Pr=\nu/\kappa$ and κ is the thermal diffusivity. $\varepsilon=1/Gr$, characterizes the degree of spatial inhomogeneity of the basic flow, and $X_g=\varepsilon X$ is the 'slow' coordinate which is used in global instability analysis.

The following forms of stream function φ_0, horizontal length scale η and temperature H_0 are proposed (subscript '0' refers to the basic flow) in order to obtain a similarity solution:

$$\varphi_0(X,Y)=2\sqrt{2}\,[1+(a-1)\varepsilon X]\,F_0(\eta), \qquad \eta=Y/\sqrt{2}, \qquad \phi_0(X,Y)=H_0(\eta). \tag{2.3}$$

Then the velocities in the boundary layer are given by

$$U_0=\frac{\partial \varphi_0}{\partial Y}=2\,[1+(a-1)\varepsilon X]\,F_0', \qquad V_0=-\frac{\partial \varphi_0}{\partial X}=-2\sqrt{2}(a-1)\varepsilon F_0. \tag{2.4}$$

Since the velocity component includes the effect of streamwise coordinate X, the present boundary-layer flow is slowly spatially developing except for a special case $(a=1)$.

Applying the boundary-layer approximation and the above transformations to equation (2.2), the steady basic flow can be described by the following ordinary differential equations:

$$\left.\begin{aligned} &F_0'''+4(a-1)F_0F_0''-4(a-1)(F_0')^2+H_0=0,\\ &\frac{1}{Pr}H_0''+4(a-1)F_0H_0'-4F_0'[1+(a-1)H_0]=0, \end{aligned}\right\} \tag{2.5a}$$

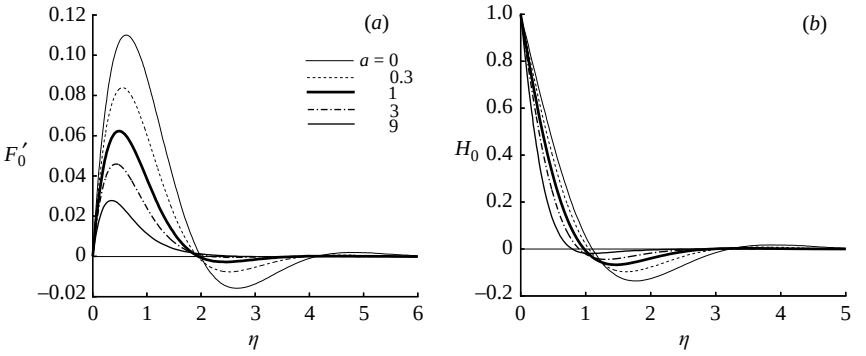

FIGURE 2. (*a*) Vertical velocity and (*b*) temperature profiles of the basic flow as functions of the temperature gradient ratio a for $Pr = 6.7$.

with boundary conditions

$$F_0(0) = F_0'(0) = 1 - H_0(0) = F_0'(\infty) = H_0(\infty) = 0. \tag{2.5b}$$

When $a = 0$ or $N = 0$, we obtain $T_w^*(x) = T_w^*(0)$; hence the wall is isothermally heated, and the above equations reduce to the ones used by Krizhevsky *et al.* (1996). When $a = 1$, the wall and the ambient fluid have the same vertical temperature gradient, consequently the horizontal velocity V becomes zero, and the flow becomes a simple parallel flow. The local heat flux dissipated from the plate can be expressed as

$$q(x^*) = -\lambda \frac{\partial T^*}{\partial y^*}\bigg|_{y^*=0} = -\frac{\lambda}{\sqrt{2}L^*}\frac{\partial H_0}{\partial \eta}\bigg|_{\eta=0} [T_w^*(0) - T_\infty^*(0)][1 + (Gr - 1)X], \tag{2.6}$$

which represents a uniform-heat-flux boundary condition as $a = 1$; λ is the conductivity of the fluid. By a simple transformation, the ordinary equations for $a = 1$ can be turned easily into the same form as discussed by Gill (1966) and Gill & Davey (1969).

Therefore, the present similarity solution makes it possible to study the effects of boundary conditions on velocity and temperature fields continuously from the uniform-heat-flux wall to the isothermal wall just by varying the temperature gradient ratio a. The ordinary equations (2.5*a*, *b*) are resolved by a fourth-order Runge–Kutta procedure and shooting method.

The cross-stream profiles of dimensionless vertical velocity $F_0'(\eta)$ and temperature $H_0(\eta)$ for different gradient ratios are shown in figure 2. In this section $Pr = 6.7$ (water) is used as an example, and the effects of Prandtl number on local and global instabilities are discussed in § 4 and § 5. It is shown that the flow reversals and temperature defects exist for both the isothermal ($a = 0$) and the uniform-heat-flux ($a = 1$) boundary conditions. Large a decreases the absolute values of the maximum and the minimum streamwise velocities, but increases the temperature gradients near the wall. Larger a means less influence of the stratified background on the flow field. It is illustrated that when $a = 9$ no flow reversal can be found in the velocity profile though the temperature defect still exists. In fact the flow reversal is difficult to find after $a > 5$ for $Pr = 6.7$.

The instability analysis is mainly focused on the transition between the two typical boundary conditions ($0 \leqslant a \leqslant 1$) and in the range $0 \leqslant \varepsilon X < 1$ ($0 \leqslant x^* < L^*$). Based on linear instability theory and the boundary-layer assumption, the governing equations (2.2*a*, *b*) are reduced to a set of linearized equations for an infinitesimal disturbance

field (see Gebhart *et al.* 1988 for a review). The following forms of disturbance stream function and temperature are introduced in these linearized equations (subscript '1' refers to disturbance field):

$$\varphi_1 = 2\sqrt{2}[1+(a-1)\varepsilon X]\Psi_1(\eta)\exp[\mathrm{i}(k_1 X - \omega_1 \tau)], \qquad \phi_1 = \Phi_1(\eta)\exp[\mathrm{i}(k_1 X - \omega_1 \tau)], \tag{2.7}$$

and then the so-called Orr–Sommerfeld equation coupled with the energy equation is obtained,

$$\left.\begin{aligned} &(\Psi_1'' - k^2\Psi_1)\left(F_0' - \frac{\omega}{k}\right) - F_0''''\Psi_1 = \frac{1}{\mathrm{i}kG}\{\Psi_1'''' - 2k^2\Psi_1'' + k^4\Psi_1 + \Phi_1''\}, \\ &\left(F_0' - \frac{\omega}{k}\right)\Phi_1 - H_0'\Psi_1 = \frac{1}{\mathrm{i}kGPr}(\Phi_1'' - k^2\Phi_1), \end{aligned}\right\} \tag{2.8a}$$

with the boundary conditions

$$\Psi_1(0) = \Psi_1'(0) = \Phi_1(0) = \Psi_1(\infty) = \Psi_1'(\infty) = \Phi_1(\infty) = 0, \tag{2.8b}$$

where

$$G = 2\sqrt{2}Gr[1+(a-1)\varepsilon X], \qquad k = \sqrt{2}k_1, \qquad \omega = \frac{\omega_1}{\sqrt{2}[1+(a-1)\varepsilon X]}. \tag{2.9}$$

The modified Grashof number, wavenumber and frequency G, k and ω are introduced only to simplify the equations. Note that in order to deduce equation (2.8*a*) the additional terms brought by the X-dependence of the disturbance stream function (2.7) are ignored as $G^{-1} \ll 1$, and this condition is satisfied well in all instability problems discussed later.

In the present work we carry out a spatio-temporal stability analysis and consequently both the modified wavenumber k and frequency ω of the disturbances are taken as complex numbers. The coordinate X_g will be considered as complex too in § 5, where the global instability is discussed. The boundary conditions at infinity are replaced by Nachtsheim's asymptotic forms at finite cross-stream distance η_{max} for numerical reasons; they were first used successfully by Nachtsheim (1963) to study natural-convection boundary-layer flows in a uniform medium. The coupled disturbance equations (2.8) are discretized with a fourth-order finite difference scheme at n uniformly distributed points in the η interval $[0, \eta_{max}]$. The resulting amplitude equations define an algebraic system $\boldsymbol{A}(\Psi_1, \Phi_1) = 0$ with sparse $2n \times 2n$ complex matrix $\boldsymbol{A}$. The homogeneous equation admits non-zero solutions for Ψ_1 and Φ_1 if and only if the determinant of $\boldsymbol{A}$

$$|\boldsymbol{A}(k, \omega, G)| = |\boldsymbol{A}(k, \omega, Gr, X_g)| = 0. \tag{2.10}$$

Based on the above relation a variable (e.g. the complex k) can be resolved by the predictor–corrector method after all the remaining variables are specified. In order to achieve numerical accuracy of the results a high enough number of points n and a large enough η_{max} must be chosen. In this paper, the result is required to vary than 0.1% when increasing by no more than η_{max} to 1.5 η_{max}. As a consequence, $\eta_{max} > 7\eta(F'_{0\,max})$ is used for all subsequent calculations. The grid point number is determined when the absolute value of the result varies by less than 10^{-8} on doubling the grid points. The numerical methods described here were tested successfully against the results of Brewster & Gebhart (1991) and Krizhevsky *et al.* (1996).

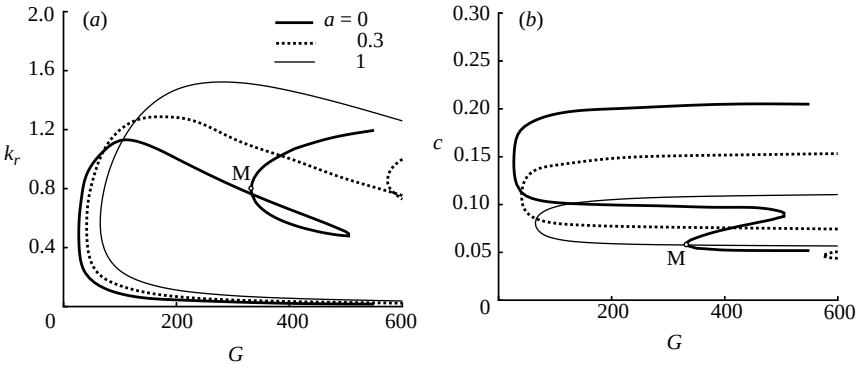

FIGURE 3. Evolution of the neutral curves for different temperature gradient ratios a in (a) the (k_r, G)-plane and (b) the (c, G)-plane for $Pr = 6.7$. The velocity $c = \omega_r / k_r$. Point M labels the critical point of mechanical instability as $a = 0$.

3. Critical instability

According to the temporal instability analysis (k real), in most cases of interest the temporal growth rate $\omega_i(k)$ reaches a maximum $\omega_{i,max} = \omega_i(k_{max})$, and this maximum growth rate is observed within the wave packet along a specific ray $X/\tau = \mathrm{d}\omega_r / \mathrm{d}k(k_{max})$. Obviously the flow is linearly unstable when $\omega_{i,max} > 0$ and linearly stable for $\omega_{i,max} < 0$. It is called neutral when $\omega_{i,max} = 0$. Several neutral curves are shown in figure 3, where the imaginary parts ω_i and k_i are zero. Similarly to the natural-convection boundary layers in a uniform medium, the neutral curves have higher and lower wavenumber parts. The higher wavenumber part apparently does not change when buoyancy effects are neglected, and this is explained by Gill & Davey (1969) as a result of mechanical instability. The lower part is a buoyancy-driven instability or thermal instability, which is caused by the coupling between the energy equation and the Orr–Sommerfeld equation. Increasing the temperature gradient ratio a enlarges the wavenumber range of unstable modes. The critical Grashof number G_c of the thermal instability is not as sensitive to a as the mechanical instability, and is just a weak function of a. Note that the 'loop' of the neutral curve in the (k_r, G)-plane (e.g. $a = 0$, figure 3a) is not a real one, but a twist in the (ω_r, k_r, G)-space (there is no 'loop' in figure 3b). Apparently, a large gradient ratio a stabilizes the boundary-layer flow, and as a result the flow around a uniform-heat-flux wall is more stable than that adjacent to an isothermal one according to the present model.

The amplitude profiles of the critical streamwise velocity and temperature disturbances are shown in figure 4. The position of the maximum amplitude moves toward the wall at higher gradient ratio a due to a thinner boundary layer. Close examination reveals that the position of the second (lower) peak in the amplitude profile of the temperature disturbance is near the location of the inflection point in the temperature profile (see figure 2b). The second peak drops with the increase of a and finally disappears when $a = 3$ (figure 4b). The two instability mechanisms also have different characteristics. For the mechanical instability the largest amplitude of the velocity disturbance lies nearly at the same position as the inflection point in the velocity profile of the basic flow, and its critical velocity (e.g. for $a = 0$ $c \approx 0.061$ at point M in figure 3b) almost coincides with the basic streamwise velocity at the inflection point. In addition, there is another peak in the near-wall region for mechanical instability, which corresponds to another critical point in the velocity profile. On

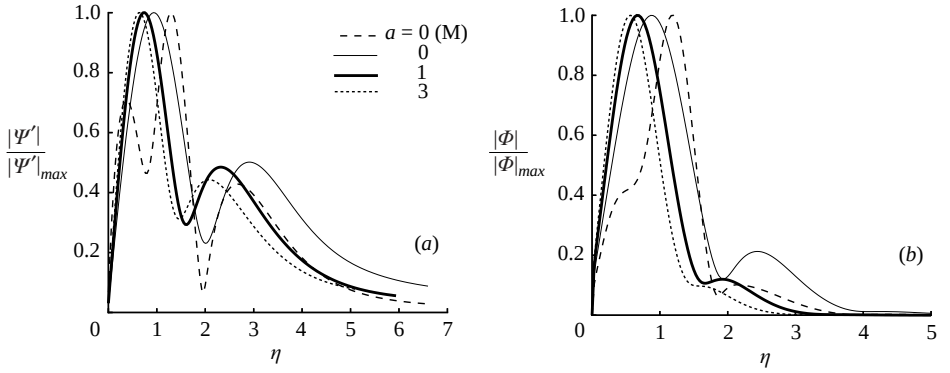

FIGURE 4. Normalized amplitude profiles of critical modes. (*a*) Velocity disturbance and (*b*) temperature disturbance for $Pr = 6.7$ and $G = G_c$. The dashed line for $a = 0$ belongs to mechanical instability, which is calculated at point M in figure 3 and used as a reference.

the other hand, for the buoyancy-driven instability the maximum amplitude of the velocity disturbance does not lie at the inflection point but at a position close to the maximum of the streamwise velocity, and no other peak values are near the wall. These differences can be explained by the fact that the critical travelling velocity (e.g. $c \approx 0.14$ for $a = 0$) is higher than the basic streamwise velocity and then no critical points exist. It is argued in §4 that the properties of the absolute instability are dominated by the mechanical instability.

4. Local absolute–convective instability transition

The Briggs–Bers criterion is used to distinguish between absolute and convective instabilities. The wavenumber observed along the ray $X/\tau = 0$ at a fixed spatial location in a laboratory frame is defined by the zero group velocity

$$\frac{\partial \omega}{\partial k}(k_0) = 0, \tag{4.1}$$

and $\omega_0 = \omega(k_0)$; $\omega_{0,r}$ is referred to as the absolute frequency and $\omega_{0,i}$ is denoted the absolute growth rate. The flow is convectively unstable (CU) if $\omega_{0,i} < 0$ and absolutely unstable (AU) if $\omega_{0,i} > 0$. Moreover, the saddle point described by equation (4.1) must be a pinching point between two distinct spatial branches $k+$ and $k-$ (k complex and ω_i constant) originating from distinct halves of the k-plane when ω_i is decreased. This condition is systematically checked in present work.

The spatial branches in the k-plane for $Pr = 6.7$ and $a = 0.1$ are shown in figure 5. When the modified Grashof number G increases from 800 to 1000, the spatial branches pinch together and interchange; simultaneously $\omega_{0,i}$ increases from -0.000197 to 0.000217. Consequently, the convectively unstable flow becomes absolutely unstable. When G increases further, it is illustrated in figure 5(*b*) that spatial branches interchange back, and $\omega_{0,i}$ decreases from 0.000168 at $G = 6000$ to -0.000102 at $G = 8000$. These results define two critical Grashof numbers G_{ca} (CU–AU) and G_{ac} (AU–CU), and imply that there is at least one maximum $(\omega_{0,i})_{max}$ in this interval. Such a flow is called type 'AF' by Monkewitz & Sohn (1986), meaning absolutely unstable with a free boundary. Flows having only one transition point or an absolutely unstable regime with a solid boundary are called type 'AB'. The AU–CU instability transition,

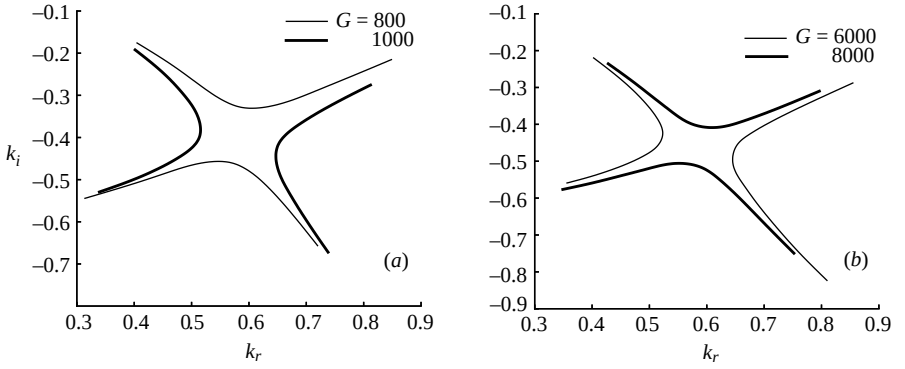

FIGURE 5. Spatial branches for $\omega_i = 0$ are contained in the complex k-plane for $Pr = 6.7$ and $a = 0.1$, (*a*) near the convective–absolute instability transition, (*b*) near the absolute–convective instability transition.

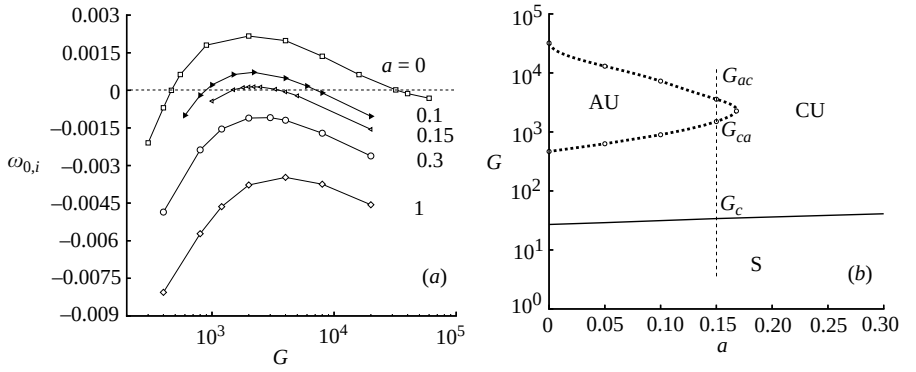

FIGURE 6. (*a*) The modified absolute growth rate $\omega_{0,i}$ as a function of G and the temperature gradient ratio a, (*b*) the convective/absolute instability boundary for $Pr = 6.7$. AU: absolutely unstable, CU: convectively unstable and S: stable.

to our knowledge, has not been reported before for any flat-plate boundary-layer flows.

It has been confirmed that some spatially developing flows (such as bluff-body wakes) with a sufficiently long streamwise interval of locally absolute instability will display time-periodic oscillations at some specific frequencies: the self-sustained global modes that are relatively insensitive to low levels of external noise. A necessary condition for linear global instability is that a finite region of local absolute instability exists within the flow field (Chomaz, Huerre & Redekopp 1988). In order to analyse the global unstable features of such a boundary-layer flow, it is necessary to study what factors affect the CU–AU–CU instability transition. Two main factors can be easily found from the basic flow governing equation (2.5): the temperature gradient ratio a and the Prandtl number.

4.1. *The effect of a*

Figure 6(*a*) illustrates that there is a single maximum $(\omega_{0,i})_{max}$ in the G interval of absolute instability. As a increases, $(\omega_{0,i})_{max}$ decreases and the critical G_{ca} increases, Consequently it becomes more difficult for the flow to be absolutely unstable. The boundary between the absolute and the convective instabilities is shown in figure 6(*b*).

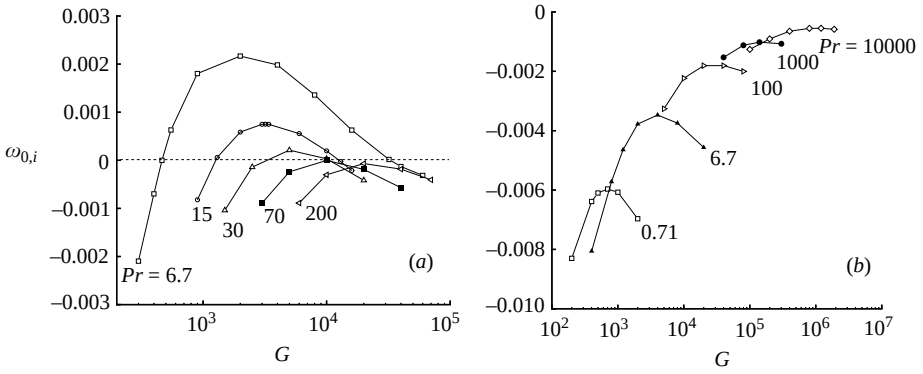

FIGURE 7. The modified absolute growth rate $\omega_{0,i}$ as a function of G for different Prandtl numbers with (a) isothermal boundary condition $a=0$, (b) uniform-heat-flux boundary condition $a=1$.

The absolutely unstable region becomes smaller at larger a, and for a larger than 0.17 the flow system does not support the absolute instability for $Pr=6.7$. Note that the uniform-heat-flux boundary condition corresponds to $a=1$. Similar effects of a on the instability transition are also obtained for other Prandtl numbers.

Krizhevsky *et al.* (1996) defined a velocity ratio, R, as the ratio between the absolute values of the minimum and maximum streamwise velocities, and found that as R increased the flow was more susceptible to absolute instability. Since smaller a leads to larger R (see figure 2a), their conclusion represents the same tendency as our results. It should be noted that the AU/CU instability transition does not always follow the CU/AU transition; it also depends on the inviscid properties of the flow, which will be discussed in § 4.3.

4.2. *The effect of Pr*

For natural-convection flows the Prandtl number should always be an important factor. Its influence on the instability is discussed for two cases: an isothermal wall ($a=0$) and a uniform-heat-flux wall ($a=1$). The evolution curves of the absolute growth rate $\omega_{0,i}$ are shown in figure 7, and two interesting changes are found as the Prandtl number increases through the values for which computations are done. Krizhevsky *et al.* (1996) found that the critical G_{ca} increased with Pr for $Pr\leqslant 40$. This result is repeated in figure 7(a). The first interesting development is that $(\omega_{0,i})_{max}$ and the interval of absolute instability decrease with the increase of Pr, and when $Pr>70$ there is no absolute instability. The second interesting feature is shown in figure 7(b). Unlike its influence on the isothermal wall, increasing the Prandtl number increases the maximum of the absolute growth rate $(\omega_{0,i})_{max}$ for the uniform-heat-flux boundary condition. However, the flow remains convective unstable even when Pr reaches as high as 10 000, where the solutions should very close to their asymptotic limits.

Just as discussed above, the convective/absolute instabilities are more complicated than was thought before for such boundary-layer flow. The boundary of the absolute–convective transition is a function of the temperature gradient ratio a, the Prandtl number and the modified Grashof number. It should be noted that the influence of Pr and G could not be combined into one factor, the Rayleigh number, it because then becomes difficult to explain the effect of Prandtl number on the absolute instability.

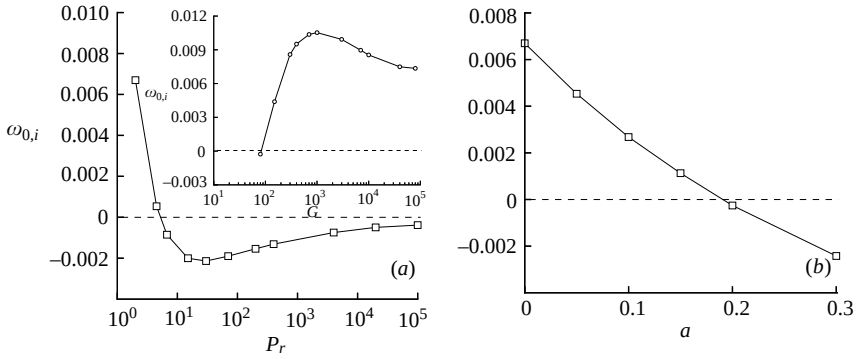

FIGURE 8. The inviscid absolute growth rate as a function of (*a*) Prandtl number Pr with isothermal boundary condition $a = 0$, and (*b*) temperature gradient ratio a for $Pr = 2$. The inset in (*a*) shows how the absolute growth rate for $Pr = 2$ and $a = 0$ closes to its inviscid limit with G.

4.3. *Inviscid limit*

When G tends to infinity and Pr remains finite, the viscous effect can be ignored and the Orr–Sommerfeld equation (2.8) will reduce to the form

$$(\Psi_1'' - k^2\Psi_1)\left(F_0' - \frac{\omega}{k}\right) - F_0'''\Psi_1 = 0, \tag{4.2a}$$

$$\left(F_0' - \frac{\omega}{k}\right)\Phi_1 - H_0'\Psi_1 = 0, \tag{4.2b}$$

together with the boundary conditions

$$\Psi_1(0) = \Psi_1(\infty) = 0. \tag{4.2c}$$

The eigenfunction Ψ_1 can be resolved from the Rayleigh equation (4.2*a*) and the boundary condition (4.2*c*) by a similar method to that used in the Orr–Sommerfeld equations, and Φ_1 can be obtained from (4.2*b*) if required. The inviscid problem is studied in this section because it allows us to determine whether the absolute instability is viscous or inviscid in origin, and to help us to understand the physical mechanism of the AU–CU transition.

It is shown in figure 8(*a*) that the inviscid absolute growth rate for the isothermal boundary condition has a minimum at $Pr = 12$, and is larger than zero when Pr is smaller than 5. Therefore, depending on the fluid properties the Rayleigh instability can be convective or absolute. The inviscid origin of convective instability predicts that when the CU–AU transition exists, the AU–CU transition is unavoidable as $G \to \infty$, and also implies that the viscous effect on the absolute instability is more crucial for fluids of larger Prandtl numbers ($Pr > 5$). When Pr is small (e.g. $Pr = 2$), it is illustrated in the inset of figure 8(*a*) that the AU–CU transition will not take place. However, as shown in figure 8(*b*), the value of inviscid absolute growth rate $\omega_{0,i}$ for $Pr = 2$ decreases with a and becomes negative when $a > 0.2$. Therefore, the basic flow can become convectively unstable even for small Pr ($Pr < 5$), provided that a is large enough.

The disturbance amplitude distributions of convective, absolute and inviscid modes are shown in figure 9. Unlike the critically convective mode, which is convected to the buoyancy-driven instability, the absolutely unstable modes are mainly dominated by mechanical instability and share some common properties with the inviscid mode: there are two critical points or two peaks in the amplitude profile separated by the

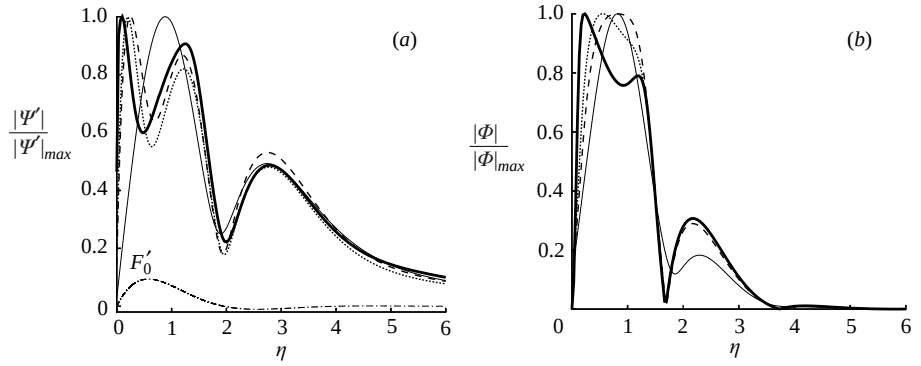

FIGURE 9. Normalized amplitude profiles of (*a*) velocity disturbances and (*b*) temperature disturbances with parameters $Pr = 6.7$ and $a = 0.15$. Thin solid line: critical mode $G = G_c$. The thick solid line, dashed and dotted lines show the corresponding solutions for the inviscid limit, $G = G_{ca}$, and $G = G_{ac}$ respectively with $(\omega, k) = (\omega_0, k_0)$. The vertical velocity profile F_0' is also shown in (*a*) as a reference (dot-dash line).

point with the largest streamwise velocity (figure 9*a*); the position of the largest amplitude of the velocity disturbance lies at the critical point near the wall. It is also illustrated in figure 9(*b*) that the position of the maximum value in the profile of the temperature disturbance moves to the location of the peak in the inviscid profile when G increases.

It has been revealed in this section that the absolute instability will appear at appropriate Prandtl number, a and the modified Grashof number G. The absolutely unstable modes reflect the influence of the Rayleigh instability, which is the asymptotic form of the mechanical instability as $G \to \infty$. The existence of absolute instability and the inviscid origin of convective instability provide the sufficient condition for the occurrence of the AU–CU instability transition.

5. Global instability

The objective of this section is to analyse the global instability of the boundary-layer flow by studying the local instability properties, which are functions of the coordinate X_g when the Grashof number Gr is fixed. For weakly non-parallel shear flows, it has been verified that the globally unstable mode is essentially connected with the local absolute instability nature, and one of the central problems regarding the global mode is the prediction of the dominant global frequency.

5.1. *Linear global instability*

The frequency selection mechanisms have been studied theoretically based on relatively simple one-dimensional evolution models such as the celebrated Ginzburg–Landau equation, and based on assumptions, e.g. the map $\omega_1(X_g)$ is single-valued and holomorphic in the complex X_g-plane (Chomaz, Huerre & Redekopp 1991). If the singularity X_{gs}, closest to the real X_g-axis of the complex function $\omega_1(X_g)$, is a saddle point, the complex frequency ω_s of the self-sustained linear global mode is given by

$$\omega_s = \omega_{10}(X_{g_s}), \qquad \frac{\partial \omega_{10}}{\partial X_g}(X_{g_s}) = 0 \tag{5.1}$$

where X_g is taken as a complex number. The medium is globally unstable whenever $\omega_{s,i} = \mathrm{Im}\omega_s > 0$.

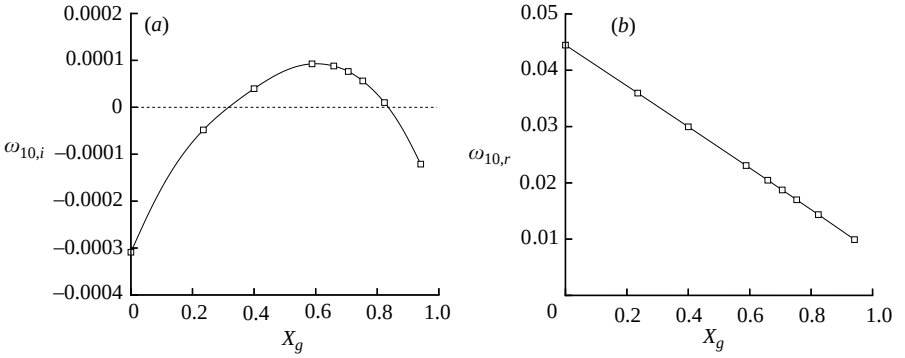

FIGURE 10. (*a*) Local absolute growth rate and (*b*) local absolute frequency as a function of streamwise station for $Pr = 6.7$, $a = 0.15$ and $Gr = 1768$ ($G = 5000$ at $X_g = 0$).

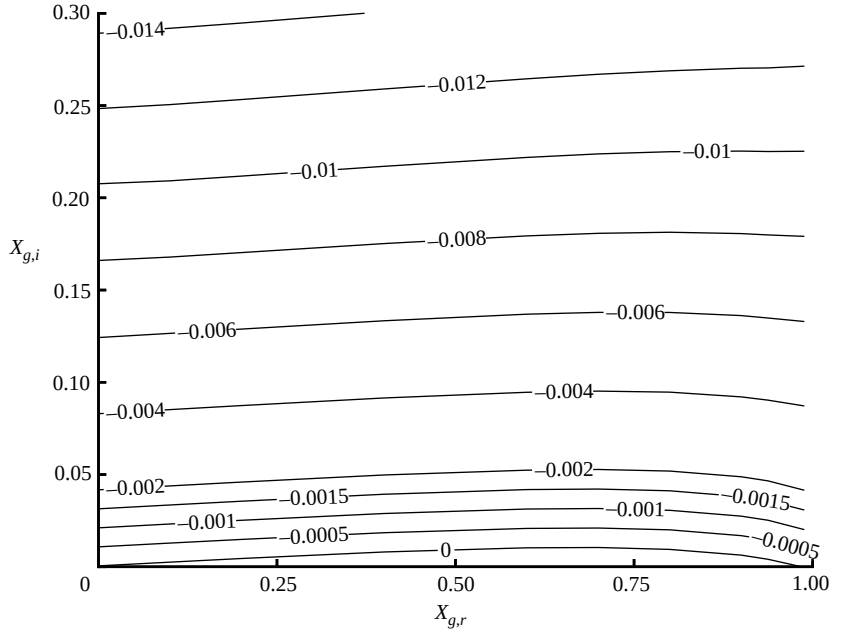

FIGURE 11. The absolute growth rate $\omega_{10,i}$ iso-contours in the complex X_g-plane for $Pr = 6.7$, $a = 0$ and $Gr = 11314$ ($G = 32000$ at $X_g = 0$).

The absolute frequency $\omega_{10,r}$ and growth rate $\omega_{10,i}$ as functions of the streamwise slow coordinate $X_g = \varepsilon X$ are shown in figure 10: $\omega_{10,i}$ reaches a maximum at about $X_g = 0.6$ while $\omega_{10,r}$ appears to decrease linearly with X_g. Since X_{gs} is the closest saddle point (if one exists) to the real X_g-axis, $X_{gs,i}$ should be very small. Usually $\omega_{10,r}$ should have a minimum at a downstream point which is very close to the position of $(\omega_{10,i})_{max}$ on the real X_g-axis, as was shown in the numerical simulation result of Hammond & Redekopp (1997). However, according to the mode described in equation (2.7) $\omega_{10,r}(X_g)$ has no minimum. As an example, the complex X_g-plane for $Pr = 6.7$, $a = 0$ and $Gr = 32\,000$ is studied. It is shown in figure 11 that the middle portion of the $X_{g,r}$-axis is on a hill whose 'altitude' is expressed in terms of $\omega_{10,i}$, but the saddle point does not exist. Another linear selection criterion of global

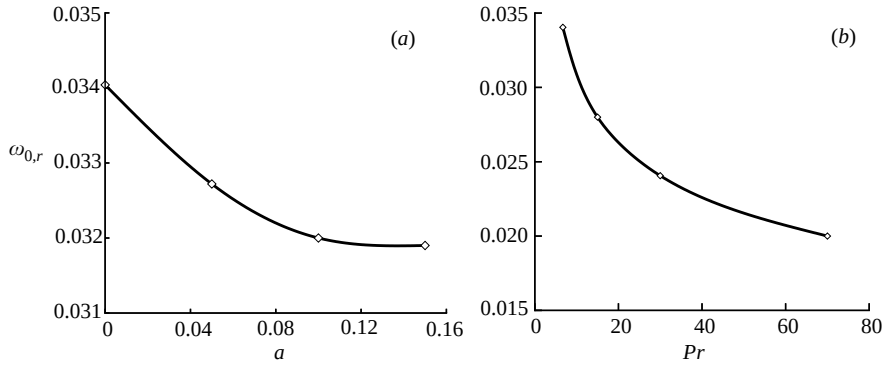

FIGURE 12. The frequency of the steep global mode ($\omega_{0,r}$ at $G = G_{ac}$) as a function of (a) temperature gradient ratio a for $Pr = 6.7$, and (b) Prandtl number for $a = 0$ (isothermal boundary condition).

frequency with an asymptotic basis is for flows of semi-infinite extent (Monkewitz, Huerre & Chomaz 1993; Woodley & Peake 1997): the global frequency ω_s is given by the upstream-boundary absolute frequency at leading order. But this criterion seems inapplicable here because of the lack of solid boundary at $X_g = 0$. Therefore, no linear frequency-selection criterion is found suitable for the present flow.

5.2. *Nonlinear global instability*

In any laboratory or numerical experiments the unstable global mode will grow from small amplitude to finite saturated patterns, and finally only for the nonlinear global mode, can the limit-cycle oscillations be observed. Dee & Langer (1983) proposed a 'marginal instability' mechanism for saturated nonlinear wave packets: the velocity of the propagating front and the wavelength of the pattern formed behind the front necessarily comply with the linear dispersion relation. By respectively numerically investigating two-dimensional parallel and spatially developing wakes, Delbende & Chomaz (1998) and Pier & Huerre (2001) recently confirmed this mechanism. By using different Ginzburg–Landau equations, Couairon & Chomaz (1997*a*, *b*) studied the nonlinear global modes in uniform semi-infinite media and found that linear absolute instability is a sufficient condition for nonlinear absolute instability. According to their results, the onset of nonlinear absolute instability coincides with the appearance of nonlinear global modes. Recently, based on a complex Ginzburg–Landau equation with slowly spatially varying coefficients, a fully nonlinear time-harmonic mode called the steep global mode was defined by Pier *et al.* (1998). Its frequency is the real linear absolute frequency at the upstream boundary of the absolutely unstable domain. Its sharp front separates an upstream decaying tail from a finite-amplitude downstream wavetrain, and just as described by the Dee–Langer selection criterion, the wavenumber at the decaying front edge coincides with the local linear absolute wavenumber. The properties of the steep global mode have been confirmed by numerical simulation results for slowly spatially developing wakes (Pier & Huerre 2001). Huerre (2000) has summarized that:

> More importantly, *steep global modes appear as soon as there exists a point of local linear absolute instability, even though the medium is still linearly globally stable*. Local linear absolute instability in a sense prevails over global linear stability and dictates the nature of the observed finite-amplitude state.

The above remark has been applied to the present system, and the frequencies of the steep global mode are shown in figure 12. Note that the 'AF' type flow cannot exist except when $G > G_{ac}$, and the most upstream absolutely unstable location lies at X_g where $G = G_{ac}$. It is shown that increasing the temperature gradient ratio a or Pr decreases the global frequencies. The amplitude distribution of the steep global mode at the trailing edge is the same as shown in figure 9 (dotted lines) for $Pr = 6.7$ and $a = 0.15$. However, the final identification of the properties of global modes depends on future experiments and direct numerical simulations.

6. Conclusion

In this work we have studied the spatio-temporal instability of the natural-convection flow around a vertically heated flat plate, where the ambient fluid and the plate have independent temperature gradients.

A similarity solution is obtained first based on a boundary-layer approximation after introducing a temperature gradient ratio a between the wall and the medium. It provides for the first time a model to study smoothly the evolution of the stability relations between the isothermal and the uniform-heat-flux boundary conditions. It is also illustrated that the flow reversal vanishes when $a > a_{crit}$ (e.g. for $Pr = 6.7$, $a_{crit} = 5$) though the temperature defect still exists. Based on an instability analysis with the coupled Orr–Sommerfeld equation and energy equation, it is shown that large temperature gradient ratio a stabilizes the flow field, and the mechanical instability is more sensitive to the variation of a than the thermal instability.

Perhaps the most important result of this paper is the discovery of the absolute–convective instability transition. The domain of absolute instability decreases with the increase of the temperature gradient ratio a. The effect of the Prandtl number on the local instability transition is also discussed. For an isothermal wall ($a = 0$), increasing Pr decreases the maximum value of the absolute growth rate $(\omega_{0,i})_{max}$, and as a result the absolute instability vanishes for $Pr > 70$. On the other hand, for a uniform-heat-flux wall ($a = 1$) larger Prandtl number leads to higher $(\omega_{0,i})_{max}$, though the growth rate remains negative in a wide Prandtl number range.

In order to gain a physical insight into this kind of flow, it is perhaps useful to summarize its instability mechanisms. When G is in the vicinity of G_c, the buoyancy-driven or thermal instability is dominant. As G is increased, the mechanical instability becomes increasingly important. The viscous effect plays an essential role in the occurrence of absolute instability for fluids of large Prandtl numbers (e.g. for an isothermal wall with $Pr > 5$). When G is very large, the main features of the unstable modes are defined by the inviscid or Rayleigh instability, and the inviscid origin of convective instability explains why the absolute–convective instability transition happens as $G \to \infty$.

Based on the local instability properties the global instability is also discussed, but no linear selection criterion for global frequency is found applicable to the boundary-layer flow according to present model. The global frequencies are determined according to nonlinear steep global mode theory. A large Prandtl number or temperature gradient ratio a tends to decrease the global frequency. The present work is intended to provide a more complete linear instability picture of this problem, and to be a basis for a subsequent fully nonlinear approach, direct numerical simulations and experiments, which can broaden our understanding of the local/global instability characteristics for such a buoyancy-driven flow system.

The research reported in this paper has been supported by French Ministry of Research and New Technologies. The authors are grateful for Dr I. Delbende's fruitful discussions.

REFERENCES

Brewster, B. A. & Gebhart, B. 1991 Instability and disturbance amplification in a mixed-convection boundary layer. *J. Fluid Mech.* **229**, 115–133.

Briggs, R. J. 1964 *Electron-Stream Interaction with Plasmas* MIT Press.

Couairon, A. & Chomaz, J.-M. 1997*a* Absolute and convective instabilities, front velocities and global modes in nonlinear systems. *Physica* D **108**, 236–276.

Couairon, A. & Chomaz, J.-M. 1997*b* Pattern selection in the presence of a cross flow. *Phys. Rev. Lett*. **79**, 2666–2669.

Chomaz, J.-M., Huerre, P. & Redekopp, L. G. 1988 Bifurcations to local and global modes in spatially developing flows. *Phys. Rev. Lett*. **60**, 25–28.

Chomaz, J.-M., Huerre, P. & Redekopp, L. G. 1991 A frequency selection criterion in spatially developing flows. *Stud. Appl. Maths* **84**, 119–144.

Dee, G. & Langer, J. S. 1983 propagating pattern selection. *Phys. Rev. Lett*. **50**, 383–386.

Delbende, I. & Chomaz, J. 1998 Nonlinear convective/absolute instabilities in parallel two-dimensional wakes. *Phys. Fluids* **10**, 2724–2736.

Gaster, M. 1968 Growth of disturbances in both space and time. *Phys. Fluids* **11**, 723–727.

Gebhart, B., Jaluria, Y., Mahajan, R. & Sammakia, B. 1988 *Buoyancy Induced Flows and Transport*. Hemisphere.

Gill, A. E. 1966 The boundary-layer regime for convection in a rectangular cavity. *J. Fluid Mech.* **26**, 515–536.

Gill, A. E. & Davey, A. 1969 Instabilities of a buoyancy-driven system. *J. Fluid Mech.* **35**, 775–798.

Hammond, D. A. & Redekopp, L. G. 1997 Global dynamics of symmetric and asymmetric wakes. *J. Fluid Mech.* **331**, 231–260.

Huerre, P. 2000 Open shear flow instabilities. In *Perspectives in Fluid Dynamics, a Collective Introduction to Current Research.* Cambridge University Press.

Huerre, P. & Monkewitz, P. A. 1990 Local and global instabilities in spatially developing flows. *Annu. Rev. Fluid Mech.* **22**, 473–537.

Iyer, P. A. 1973 Instabilities in buoyancy driven boundary layer flows in a stably stratified medium. *Boundary-Layer Metel.* **5**, 53–66.

Iyer, P. A. & Kelly, R. E. 1978 Supercritical solutions for the buoyancy boundary layer. Trans. *ASME: J. Heat Transfer* **100**, 648–652.

Jaluria, Y. & Gebhart, B. 1974 Stability and transition of buoyancy-induced flows in a stratified medium. *J. Fluid Mech.* **66**, 593–612.

Jaluria, Y. & Himasekhar, K. 1983 Buoyancy-induced two-dimensional vertical flows in a thermally stratified environment. *Comput. Fluids* **11**, 39–49.

Krizhevsky, L., Cohen, J. & Tanny, J. 1996 Convective and absolute instabilities of a buoyancy-induced flow in a thermally stratified medium. *Phys. Fluids* **8**, 971–977.

Kulkarni, K., Jacobs, H. R. & Hwang, J. J. 1987 Similarity solution for natural convection flow over an isothermal vertical wall immersed in thermally stratified medium. *Intl J. Heat Mass Transfer* **30**, 691–698.

Monkewitz, P. A., Huere, P. & Chomaz, J.-M. 1993 Global linear stability analysis of weakly non-parallel shear flows. *J. Fluid Mech.* **251**, 1–20.

Monkewitz, P. A. & Sohn, K. D. 1986 Absolute instability in hot jets and their control. *AIAA Paper* 86–1882.

Moresco, P. & Healey, J. J. 2000 Spatio-temporal instability in mixed convection boundary layers. *J. Fluid Mech.* **402**, 89–107.

Nachtsheim, P. R. 1963 Stability of free-convection boundary layer flows. *NACA TN* D-2098.

Pier, B. & Huerre, P. 2001 Nonlinear self-sustained structures and fronts in spatially developing wake flows. *J. Fluid Mech.* **435**, 145–174.

Pier, B., Huerre, P., Chomaz, J. & Couairon, A. 1998 Steep nonlinear global modes in spatial developing media. *Phys. Fluids* **10**, 2433–2435.

Prandtl, L. 1952 *Essentials of Fluid Dynamics*, pp. 422–425. Blackie, London.

Tao, J. & Zhuang, F. 2000 Absolute and convective instabilities of the natural convection in a vertical heated slot. *Rhys. Rev.* E **62**, 7957–7960.

Woodley, B. M. & Peake, N. 1997 Global linear stability analysis of thin aerofoil wakes. *J. Fluid Mech.* **339**, 239–260.